

Mode of crustal extension determined by rheological layering

C. Wijns, R. Weinberg, K. Gessner, L. Moresi

Abstract

Pre-existing structures and weaknesses are often thought to control the behaviour of continental crust under extension. While such features do play a role, the mechanical stratification of the crust can also dominate the mode of extension. In our numerical models, the temperature gradient dictates the transition from a strong, brittle, upper crust to a weaker, ductile, lower crust. Results show two distinct extension modes that depend upon this vertical rheological contrast: the *distributed faulting mode* and the *metamorphic core complex mode*. In the absence of pre-existing weaknesses, the ratio of the integrated strength of the upper to lower crust is an indicator of the resulting mode of extension. When this strength ratio is small, i.e., the lower crust is relatively strong, the result is distributed, densely spaced faulting, with limited slip on each fault, and no exposure of lower crustal rocks. An example could be faulting in the North Sea. A large strength ratio, hence a weak lower crust that flows easily, leads to stretching being strongly localised onto relatively few normal fault zones. Each fault accommodates large displacements, eventually dissecting the upper crust and resulting in exhumation of the lower crust. This is representative of the metamorphic core complexes of the Western U.S.A. and the Aegean. The actual critical strength ratio for the transition between modes will depend upon secondary factors such as the relative thickness of the lower crust with respect to the upper crust, and the degree of fault weakening.

1 Introduction

Continental lithosphere may be highly extended without entirely rifting to a new ocean basin. For example, total Cenozoic strain estimates (β factors) of up to 2 have been proposed for parts of the Basin and Range in the western U.S.A., which has not been rifted [e.g., *Lachenbruch and Sass, 1978; Jones et al., 1992*]. A total of up to 80% extension is suggested on a very large scale of 300–500 km [*Wernicke et al., 1982*], and *Niemi et al. [1999]* have even suggested 500% extension in central Death Valley, California, since the middle Miocene. Stretching of the crust may then be accommodated by two contrasting phenomena: distributed, closely spaced, and limited-slip normal faulting over a large area, or localised, large-strain normal faulting that often results in the complete dissection of the upper crust and exhumation of the lower crust. Examples of distributed faulting exist in various parts of the North Sea basin [e.g., *Fossen and Rørnes, 1996; Viejo et al., 2002*], where the faults are characterised by a relatively steep angle and small offset. Normal faults that exhibit a low angle and very large displacement, juxtaposing exhumed high-grade metamorphic rocks against near-surface rocks, are hallmarks of the metamorphic core complexes (*mcc*) of the Basin and Range [e.g., *Axen et al., 1990; Duebendorfer et al., 1990; Hodges et al., 1990; Spencer and Reynolds, 1991*] or the Aegean [e.g., *Gauthier and Brun, 1994; Burchfiel et al., 2000; Gessner et al., 2001*].

Why should extending lithosphere sometimes form an *mcc* in preference to failing in a distributed manner? One possibility is that major lateral discontinuities in the strength of either the upper crust (e.g., pre-existing faults) or the lower crust (e.g., partial melt zones) focus stresses and localise extension. *Christiansen and Pollard [1997]* have documented field evidence for the nucleation of shear zones

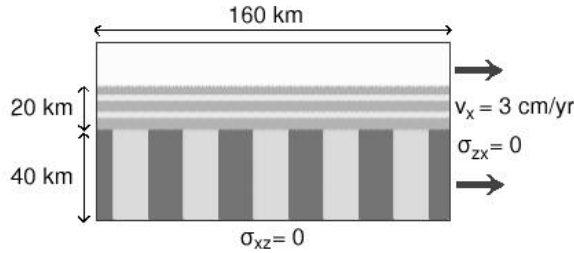


Figure 1: Initial geometry and boundary conditions for the numerical models. Stripes in the upper and lower crust are marker materials for visualising deformation. All bounding surfaces have zero shear stress, and the box is extended from the right-hand side. Vertical boundaries have zero heat flux, i.e., are reflective.

from pre-existing dikes acting as weaknesses, although these were not associated with an *mcc*. In their conceptual models of extensional tectonics, both *Wernicke* [1985] and *Wernicke and Axen* [1988] assume an immediately active horizontal or low-angle detachment surface through the upper crust, which then controls faulting and exhumation of the lower crust. In some analogue modelling experiments, initial faults end up controlling fault spacing and the mode of extension [e.g., *Koyi and Skelton*, 2001]. *Brun et al.* [1994] conclude that a weak rheological zone at the base of the upper crust is required to trigger an *mcc*. Other analogue modellers use a weak zone in the upper mantle combined with an imposed velocity discontinuity [*Corti et al.*, 2001], or a pre-weakened lower lithosphere [*Mulugeta and Ghebreab*, 2001], such that stresses are localised and influence the resulting extension. Some numerical modelling experiments also suppose initial weaknesses, and proceed to investigate related factors that vary the results of extension [e.g., *Dunbar and Sawyer*, 1989]. Although such weak features do serve to focus stresses, we find that in the absence of lateral heterogeneities, vertical contrasts in rheology dictate whether one or the other mode of extension will result. In fact, small lateral heterogeneities are often insufficient to trigger an *mcc* mode when the rheological layering promotes distributed faulting.

The mode of extension is thus determined by the combined ability of both lateral and vertical rheological structure to focus stresses in the brittle upper crust. Our numerical modelling concentrates on the role of the vertical rheological contrast in dictating the spacing between fault zones and the accompanying mode of distributed faulting or *mcc* formation. Numerical models have the advantage over analogue experiments of exact control over “laboratory” conditions, and precise specification of rheological behaviour and initial and boundary conditions. On the other hand, given the level of readily-available computational power today, numerical models still lack the resolution of analogue models, especially in three dimensions. Thus we confine ourselves to 2D vertical section models, which, fortunately, are easily compared to much published analogue modelling, including that of *Brun et al.* [1994].

2 Models

We use a two-dimensional Lagrangian integration point finite element code [*Moresi et al.*, 2001, 2002] to explore the different behaviours of the crust during extension. The algorithm solves the governing equations of momentum, mass, and heat conservation. Inertial terms are neglected. The particle-in-

cell approach allows simulations to develop very large strains comparable to those found in analogue models, while still tracking strain history accurately for the constitutive laws. Examples of geological and engineering problems are on the World Wide Web at <http://www.ned.dem.csiro.au/research/solidMech/PIC>, and in *Moresi and Lenardic* [1999], *Mühlhaus et al.* [2001], and *Mühlhaus et al.* [in press, 2002].

We consider viscoplastic materials with strain-weakening behaviour, which gives rise to the localisation of deformation and necking of layers. A yield law approximates brittle behaviour in the strong upper crust, which overlies a weaker, ductile lower crust. The transition from brittle to ductile behaviour is governed by temperature. The initial geometry of the model appears in Figure 1, and corresponds to 20 km of upper crust atop 40 km of lower crust, along a length of 160 km. Horizontal stripes in the upper crust and vertical stripes in the lower crust are simply marker materials to enhance visualisation of the deformation. The pattern is copied directly from *Brun et al.* [1994]. Above these two crustal layers is a highly compressible layer of low viscosity, low density, background material (“air”), which does not interfere with the mechanics of the problem. Vertical walls of the closed bounding box are free-slip. Extension proceeds by applying a uniform velocity to the right-hand boundary, equivalent to 100% strain in 5 Ma [*Gessner et al.*, 2001], or $6.3 \times 10^{-15} \text{ s}^{-1}$. This boundary velocity does not create tensional stresses, so gravity is in effect driving the deformation.

The yield law for the upper crust prescribes a maximum shear stress τ_{yield} , calculated via the second invariant of the deviatoric stress tensor, according to

$$\tau_{\text{yield}} = (c_o + c_p p) f(\varepsilon) \quad (1)$$

where p is the pressure, c_o is the cohesion, or yield stress at zero pressure, and c_p is the pressure dependence of the yield stress, equivalent to the friction coefficient in Byerlee’s law [*Byerlee*, 1968]. We adopt a low rock cohesion of 16 MPa [*Suppe*, 1985, p. 155], which is greater than the value of zero employed in Byerlee’s law for the upper 10 km of the crust, but avoids a cohesionless surface material that would allow plastic strain along the entire air-rock interface. Numerous laboratory experiments by *Byerlee* [1968] resulted in a universal friction coefficient of 0.6 – 0.85 for most rock types. However, this is for dry samples. Assuming an average hydrostatic pore pressure, the effective pressure is reduced by more than one third, so that an equivalent dry friction coefficient of 0.7 is reduced to 0.44. Strain-weakening is included through the power law function $f(\varepsilon)$, in which ε is the accumulated plastic strain, measured as the second invariant of the deviatoric strain tensor.

$$f(\varepsilon) = \begin{cases} 1 - (1 - a) (\varepsilon/\varepsilon_o) & \varepsilon < \varepsilon_o \\ a & \varepsilon \geq \varepsilon_o \end{cases}$$

The “saturation” strain ε_o is the accumulated plastic strain beyond which no further weakening takes place, and at this point the maximum proportion of strain weakening is given by a . There is no strain weakening when $a = 1$. Both of these parameters are varied in order to investigate the influence of fault weakening on the mode of extension.

The boundary between upper and lower crust is defined at all times by a fixed density contrast. Initially, this corresponds to the depth at which the temperature dictates a change from brittle to ductile behaviour. With increasing extension, the initially Newtonian lower crust may be exhumed into the brittle field and undergo faulting. It behaves mechanically as the upper crust does, but retains the density

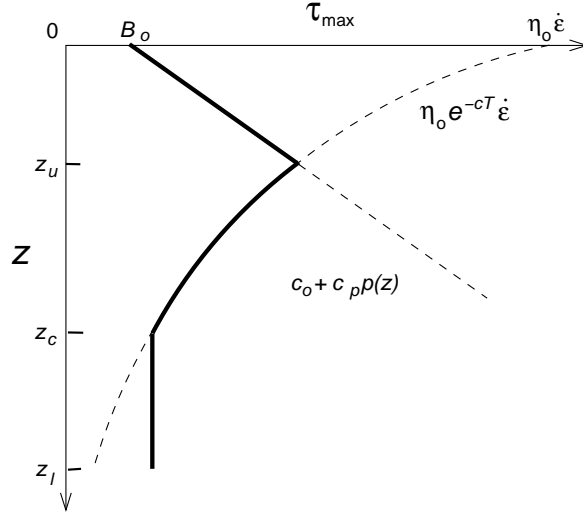


Figure 2: Representative maximum shear stress profile (solid line) through the crust for a given strain rate $\dot{\epsilon}$. Neglecting localised strain weakening, strength increases with pressure p from c_0 at the surface to a maximum value at the base z_u of the brittle upper crust, at which point the yield curve intersects the viscous, temperature-dependent flow law. The viscosity value at z_c is adopted as a minimum value and is constant to the base z_l of the crust.

(and, e.g., metamorphic grade and mineralogy) of lower crustal material. We do not consider any thermal expansion, since, during exhumation, we expect decompression to compensate for cooling; nor do we model melting.

Viscosity η varies with temperature T according to the Frank-Kamenetskii relation [Frank-Kamenetskii, 1955]

$$\eta(T) = \eta_0 e^{-cT} \quad (2)$$

This is a simplification of an Arrhenius rheology, where the constants η_0 and c are chosen such that the viscosity at the interface z_u between upper and lower crust, which is the initial brittle to ductile transition, satisfies the maximum yield stress

$$\tau_{\text{yield}}(z_u) = \eta(T(z_u)) \dot{\epsilon}$$

i.e., the maximum shear stress profile through the crust is continuous. Appendix B contains a full development of these relations, and Figure 2 illustrates a crustal strength profile. The profile evolves with the strain rate, but provides a convenient starting point from which to characterise the crust.

The surface of the upper crust is maintained at 0°C . An initial temperature gradient of $20^\circ\text{C}/\text{km}$ results in a brittle to ductile transition at 400°C , in the range discussed by *Brace and Kohlstedt* [1980] and references therein, *McKenzie and Fairhead* [1997], and corresponding to theoretical flow laws derived by *Handy et al.* [1999] for various crustal components. At this depth, the maximum shear strength of the crust is about 250 MPa. Because of the significant initial thickness of the crust, the base of the model reaches a constant temperature of 1200°C , which is probably too high. However, since the temperature only controls the viscosity of the lower crust, we avoid an extremely low viscosity by limiting $\eta(T) > \eta(T = 600^\circ\text{C})$.

Parameter	Value
thickness z_u , upper crust	20 km
thickness $z_l - z_u$, lower crust	40 km
velocity U , boundary	3.1 cm/yr
strain rate $\dot{\epsilon}$, initial	$6.3 \times 10^{-15} \text{ s}^{-1}$
density ρ_u , upper crust	2700 kg/m^3
density ρ_l , lower crust	3000 kg/m^3
gravity g	10 m/s^2
cohesion c_o	16 MPa
friction coefficient c_p	0.44
strain weakening a , maximum	0.2
“saturation” strain ϵ_o	0.5
thermal diffusivity κ	$10^{-6} \text{ m}^2/\text{s}$
temperature T_s , surface	0°K
temperature T_b , base	1200°K

Table 1: Natural parameter values.

Table 1 contains parameter values for the natural system, which apply to all models unless explicitly stated otherwise. The scaling equations that translate these into model values are contained in Appendix A.

3 Results

In all of the following simulations, bands of high localised plastic strain represent fault zones. Accumulated plastic strain in the upper crust is indicated by darkened material, and the degree of shading is indicative of the amount of strain. Faults form at 33° to the direction of greatest principal stress, corresponding to an angle of internal friction $\tan^{-1}c_p = 23^\circ$. Unless otherwise indicated, a maximum of 80% strain weakening ($a = 0.2$) occurs after an accumulated strain $\epsilon_o = 0.5$. These values reflect evidence, from both numerical experiments [e.g., *Bird and Kong*, 1994] and field-based heat-flow measurements [e.g., *Lachenbruch and Sass*, 1980, 1992], that major faults may undergo significant weakening.

The different behaviours of the crust under extension are partly parameterised by the ratio r_τ of integrated upper to lower crustal strength. The calculation of integrated strengths, based on the maximum sustainable shear stress at a given strain rate, is explained in Appendix C.

3.1 Constant viscosity

The two contrasting modes of crustal extension are first illustrated in Figures 3 (model A, distributed faulting) and 4 (model B, *mcc*) for a constant viscosity lower crust. A constant viscosity is the only feasible approach for analogue modelling, and allows us to compare directly with the results of *Brun et al.* [1994]. When the lower crust has a relatively high viscosity, i.e., the system is characterised by a small r_τ , the result is the distributed faulting in Figure 3. The upper crust develops many closely spaced steep faults, each of which accommodates a limited strain, and the interface between upper and lower crust remains relatively flat. This is very similar to the equivalent model of *Brun et al.* [1994]. Even with stretching $\beta > 1.8$ shown here, the upper crust is never completely dissected. New steep faults form

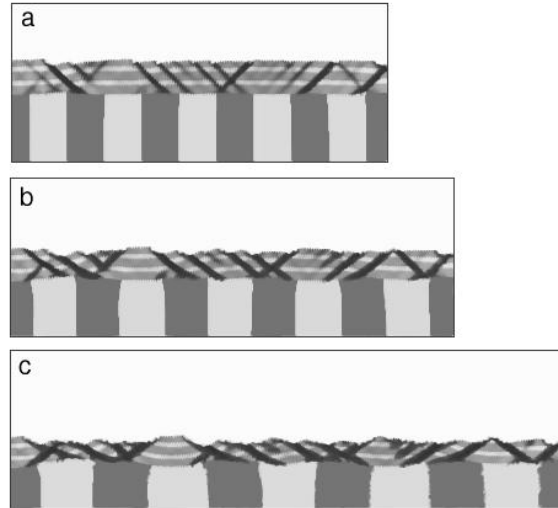


Figure 3: Model A: evolution of distributed faulting mode with a lower crust of constant viscosity and $r_\tau = 0.53$. Total extension of (a) 24% (1.2 Ma), (b) 52% (2.6 Ma), and (c) 82% (4.1 Ma). Dark bands in the upper crust indicate accumulated plastic strain, or fault zones.

soon after older faults have accommodated a small amount of shear strain, with the end result that the upper crust is broken into a series of small blocks. For this example $r_\tau = 0.53$.

Although *Brun et al.* [1994] propose that a weakness is needed in the lower crust in order to localise stresses and trigger an *mcc* mode of extension, we show in model B (Figure 4) that a uniformly weak lower crust, i.e., a high $r_\tau = 2.52$, is sufficient to achieve this behaviour. Deformation is accommodated by only a few normal fault zones. Displacement is large within each fault zone, which furthermore remains active even after rotating to a shallow dip, because of fault weakening. The lower crust flows easily to isostatically compensate for localised thinning of the upper crust, which enhances block rotation and continued strain on low-angle faults. The lower crust is first exhumed at $\beta = 1.6$.

3.2 Temperature dependent viscosity

The main limitation in using a constant viscosity for the lower crust, and therefore a limitation of the analogue modelling, is that lower crustal material that rises towards the surface remains very weak, although it should cool and strengthen, even becoming brittle. This phenomenon does not affect the case of distributed faulting, where the lower crust remains buried below a laterally stable brittle to ductile transition. In model A, the interface between upper and lower crust remains between 400°C and 450°C . In *mcc* mode, however, a temperature dependent viscosity allows exhumed lower crust to realistically cool and enter the brittle domain. The relative rate of cooling versus exhumation will influence *mcc* formation.

A weak lower crust in a laterally uniform system still results in the *mcc* mode of extension in Figure 5 for $r_\tau = 2.15$. The rising lower crust enters the brittle domain, but cooling is slow enough, relative to exhumation, that brittle deformation of the lower crust does not penetrate to great depth. The propagation of faults from the upper crust into the lower crust allows continued strain along the original structures,

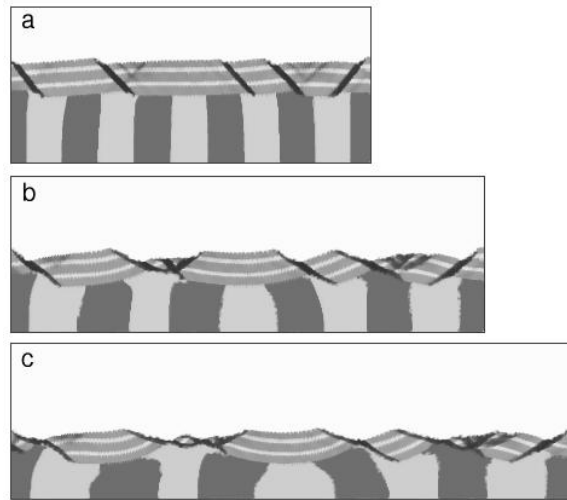


Figure 4: Model B: evolution of *mcc* mode caused by a uniformly weak lower crust of constant viscosity and $r_\tau = 2.52$. Total extension of (a) 25% (1.2 Ma), (b) 53% (2.7 Ma), and (c) 83% (4.2 Ma).

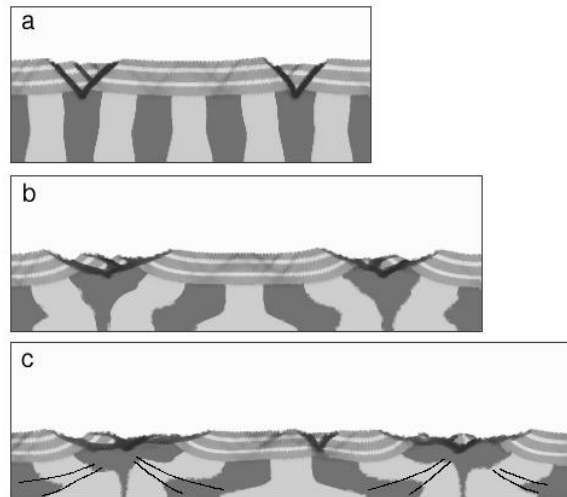


Figure 5: Model C: evolution of *mcc* mode ($r_\tau = 2.15$) with both a viscosity and a brittle to ductile transition that are temperature dependent. Total extension of (a) 16% (0.8 Ma), (b) 53% (2.6 Ma), and (c) 82% (4.1 Ma). Faults continue to propagate through the newly brittle lower crust as it nears the surface, and are connected to diffuse high shear zones in the ductile region, indicated with pairs of solid lines in (c).

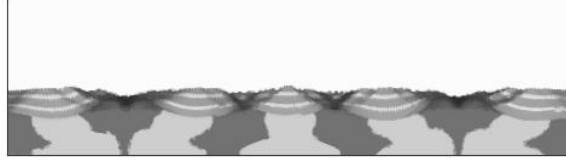


Figure 6: Model E: *mcc* mode with $r_\tau = 2.15$, but a maximum fault weakening of 20% rather than 80% as in model C. Total extension of 80% (4.0 Ma).

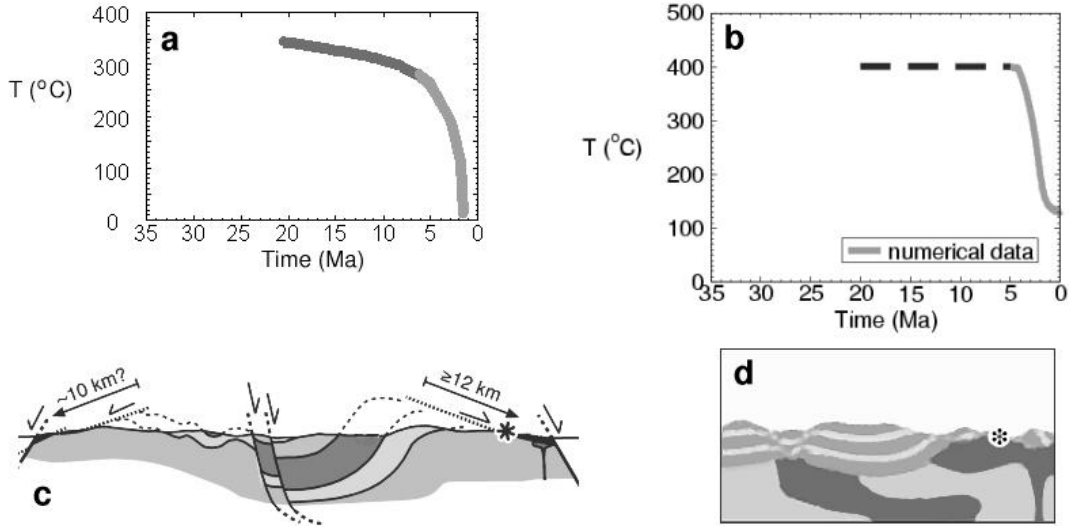


Figure 7: Temperature-time path for an exhumed footwall of an *mcc* from (a) fission-track thermochronology and $\text{Ar}^{40}/\text{Ar}^{39}$ ages (from Gessner *et al.* [2001]) and (b) numerical model C. The dotted line in (b) represents the initial stable temperature before the onset of extension. (c) Schematic cross section of Central Menderes *mcc* from Gessner *et al.* [2001]. The asterisk denotes the location, in high grade metamorphic material, of the laboratory analyses. (d) Part of model C *mcc* with an asterisk showing the equivalent (final) location of numerical temperature sampling point.

until they become very gently dipping or even flat-lying detachment surfaces accommodating large displacements. There is evidence in the vertical lower crust markers that these faults are spatially connected to diffuse high shear zones that extend to the base of the entire crust. These deep shear zones are traced in Figure 5c. Such continuity has been suggested in an intraplate setting by Zoback *et al.* [1985].

In order to determine the importance of fault weakness with respect to *mcc* formation, we have modified model C to severely restrict the amount of strain-weakening. Model D has a maximum strain-weakening of only 20% ($a = 0.8$), and this accumulates more slowly through $\varepsilon_o = 1.0$. The resulting extension still produces an *mcc* mode, although the characteristics are different (Figure 6). Fault zones are more diffuse and the upper crust tends to neck rather than produce planar shear zones.

3.3 Field validation

We test the physical validity of the *mcc* model C by comparing our numerical results with cooling data from the Kuzey detachment in the Central Menderes. After 100 % extension, the crust is approximately

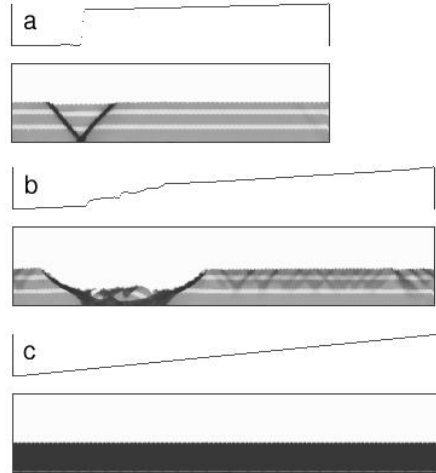


Figure 8: (a) Endmember of *mcc* mode ($r_\tau \rightarrow \infty$) represented by the brittle upper crust atop a free-slip lower boundary. Total extension of 3% (0.15 Ma). The profile above is the normalised basal velocity. No other yielding will occur because the strain rate approaches zero away from the first developed fault (graben). (b) Same model as (a) at a total extension of 38% (1.9 Ma). Because the code cannot model actual discontinuities, there is some stress transmitted across the graben. At this stage, gravitational slumping also begins to affect the model because there is no lower crust isostatic compensation. (c) Endmember of distributed faulting mode ($r_\tau \rightarrow 0$) represented by the brittle upper crust atop a zero-slip boundary. Total extension of 40% (2.0 Ma). A very strong lower crust ensures uniform basal traction (reflected in the velocity profile above), which leads to uniform yielding of the upper crust.

30 km thick, which coincides with a seismic investigation of western Turkey by *Saunders et al.* [1998]. The numerical temperature-time curve in Figure 7b matches well, with respect to the rate of temperature decay, with data from *Gessner et al.* [2001] and *Hetzel et al.* [1995] (Figure 7a). Both data sets are from the exhumed footwall of an *mcc*. The field data reflect measurements from apatite and zircon fission-track thermochronology, and $^{40}\text{Ar}/^{39}\text{Ar}$ ages for the higher temperatures. There is a 100°C offset in initial temperatures due to our chosen starting conditions. Furthermore, the numerical curve does not reach the surface temperature of 0°C because, due to the continuum nature of the code, the upper crust is never completely removed from above the exhumed lower crust, so that the lower crust remains buried and begins to stabilise at approximately 100°C .

The match we have achieved between cooling rates for the numerical and field data suggest that the model formulation provides an adequate physical description for our investigation of extensional tectonics.

4 Discussion

Pre-existing faults or thermal and rheological heterogeneities are not required to produce an *mcc* mode of extension. A large ratio of upper to lower crustal strength is sufficient. As the ratio r_τ is further increased, we reach a state where a single fault is nucleated and remains the only zone of failure. This is illustrated by the endmember case $r_\tau \rightarrow \infty$ of a single brittle layer extended over a free-slip lower boundary, as in Figures 8a and b. Once a fault or symmetric graben is nucleated, boundary stresses can

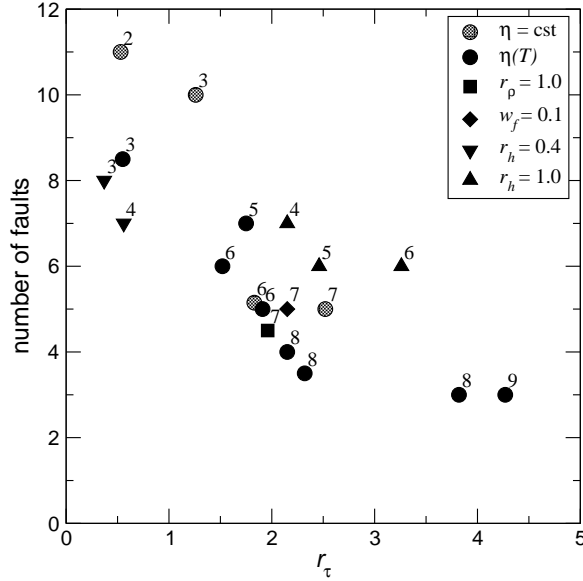


Figure 9: Number of major fault zones as a function of r_τ . Data labels indicate a subjective evaluation of the model result between the distributed endmember (0) and the *mcc* endmember (10). Unless otherwise indicated, viscosity η is temperature dependent, $r_h = 0.5$, $r_\rho = 0.9$, and $w_f = 0.53$. The influence of both density contrasts r_ρ (at this strain rate) and fault weakening w_f are clearly minor compared to the control exerted by r_τ . Differences due to crustal thickness ratios r_h are more pronounced.

no longer be communicated laterally through the layer, and the velocity gradient approaches zero away from the fault, as evidenced by the basal velocity profile above the section. This is the limit of very weak lower crust that effectively decouples the upper crust from the tectonics below. If the fault was truly a discontinuity (impossible with this continuum code), the velocity gradient would be zero everywhere except at the discontinuity, unlike the profile in Figure 8b, where some stress continues to be transmitted. The lower crust, when present, fulfills the role of stress distributor and ensures non-zero traction at the base of the brittle crust. When the lower crust is so strong as to maintain a constant stress at this interface, $r_\tau \rightarrow 0$ and we have the zero-slip basal condition illustrated in Figure 8c. The result, uniform yield of the upper crust, is the endmember of distributed faulting.

The $r_\tau \rightarrow \infty$ model in Figure 8b will not necessarily result in *mcc* formation. The presence of a volume of mobile lower crust may be essential for block rotation, shallowing of fault dips, and lower crust exhumation. Fault zone localisation and significant block rotation are complementary expressions of the weak lower crust endmember. These two phenomena might not be separable in nature.

The number of major fault zones that are developed to accommodate extension correlates inversely with the tendency to *mcc* mode. The dependence of mode on r_τ is illustrated in Figure 9, using the number of major fault zones as a proxy for the mode of extension. Fewer fault zones develop with increasing r_τ . More models have been run than are shown in the previous section, in order to explore the phase space of extension modes. Models are labelled with a subjective rank from 0 to 10, corresponding to position between the endmembers of, respectively, distributed faulting and *mcc* mode. In addition to r_τ , the following parameters simplify model classification: the ratio r_h of upper to lower crust thickness,

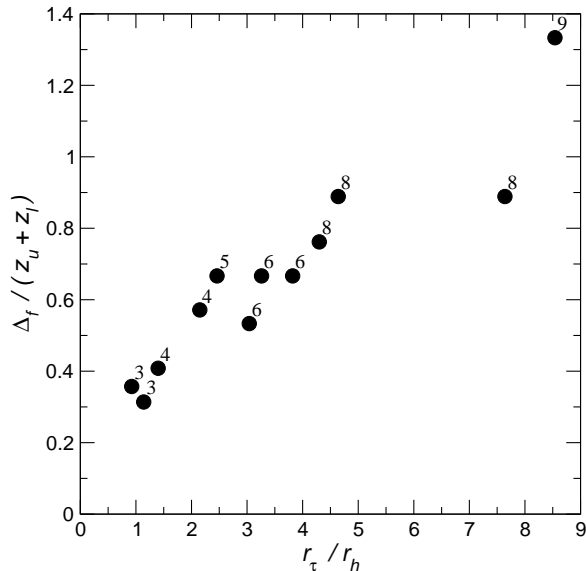


Figure 10: Spacing Δ_f of major fault zones (normalised by total crustal thickness $z_u + z_l$) as a function of r_τ/r_h for temperature dependent models only. All data points have $r_\rho = 0.9$ and $w_f = 0.53$. Data labels indicate mode as in Figure 9. The trend should pass through the origin and towards infinite spacing for $r_\tau/r_h \rightarrow \infty$, although these cases would not be reached for natural parameter ranges for the crust.

the ratio r_ρ of upper to lower crust density, and the fault weakness factor $w_f = (1 - a)/(1 + \varepsilon_o)$. A larger w_f implies greater and/or more rapid fault weakening. According to Figure 9, variations in r_τ exert the greatest control on the mode of extension. Of secondary but significant importance is r_h , while r_ρ and w_f have a minor influence. The extension rate in these models may be too high for density contrasts to appreciably affect exhumation of the lower crust. Buoyancy forces will be more evident for lower extension rates, at some point dictating a transition to diapirism for $r_\rho > 1$.

When the different thickness ratios r_h are accounted for, the standard deviation of model behaviour is largely reduced. Figure 10 shows the more or less linear variation between normalised fault spacing and r_τ/r_h . Only temperature dependent models with $r_\rho = 0.9$ and $w_f = 0.53$ are included. This simplistic relationship is a purely empirical prediction of model behaviour, within the assumptions of our initial conditions. Other physical formulations for the models may change the absolute values of our defining parameters, but we have shown that there exists a continuum of behaviour in extension that depends mostly upon the contrast between upper and lower crustal strength. Furthermore, after significant extension ($\beta > 1.8$), we have found only two endmember modes. A small r_τ results in a contiguous upper crust even after extreme stretching, whereas a large r_τ initiates more localised strain that evolves into an *mcc*.

There is no upper mantle in our models, which precludes direct comparison with the modes of extension of *Buck* [1991]. However, an equivalent “narrow rift” mode in our models is simply a juvenile *mcc* mode in terms of total extension. Strain is localised in one or few zones, but the lower crust is not yet exhumed. Analogue modelling by *Benes and Davy* [1996] purports to support the modes of *Buck* [1991], in which they use a similar measure of layer strength ratios as we do to distinguish model be-

haviour. They conclude that very weak lower crust gives rise to an *mcc* mode of extension, and our results are broadly consistent with theirs. While *Benes and Davy* [1996] also classify a narrow rift mode, they change the upper to lower crust thickness ratio with respect to their core complex models to achieve this. A narrow rift, which they classify after only 9.3% extension, is the result of a thicker upper crust and a thinner lower crust, which both contribute to hindering exhumation of the lower crust. A thick upper crust simply requires more strain until it is dissected. A thin lower crust, relative to a thick lower crust, relies more on lateral flow to compensate for unloading, and thus, at the same integrated viscosity, does not as easily accommodate an *mcc* mode of extension. We suspect that given greater extension, the narrow rifts of *Benes and Davy* [1996] are actually core complexes, whereas the “wide rifts” will remain as such, equivalent to our distributed faulting models. Narrow rifts are an intermediate mode and not an endmember behaviour.

The upper mantle will have some influence on the behaviour of the crust during extension. The thinner or stronger the lower crust, the more likely this influence will manifest itself. The lower crust in our models is sufficiently thick and ductile that it effectively decouples the crust from the upper mantle. If the upper mantle is strong, it will then remain relatively flat, as the lower crust will flow more quickly in response to any unloading. This case is implicit in our use of a rigid, zero-traction bottom boundary, and corresponds to the observations of a flat moho boundary under areas of high extension in Arizona [*Hauser et al.*, 1987]. On the other hand, if the upper mantle is of comparable viscosity and subject to flow on the same time scale as the lower crust, it will participate in isostatic compensation. With the thick lower crust geometry of our present modelling, however, we do not envisage that inclusion of the upper mantle will change the basic conclusion with respect to the importance of upper to lower crustal strength ratios in controlling the mode of extension. On a larger scale, the upper mantle, in concert with the lower crust, most likely plays a crucial role in continental breakup.

Some field vindication of the case for weak lower crust promoting *mcc* formation might be argued based on work by *Parsons et al.* [2000]. A seismic low-velocity middle crust (hotter and/or weaker) is present under the Buckskin-Rawhide core complex in Arizona, U.S.A. Further west there is high-velocity middle crust (colder and/or stronger) under the steep normal faults of the Salton Trough.

To explain why strength contrasts may control the mode of extension, we turn to numerical work by *Bai and Pollard* [2000] that explains fracture spacing in layered rocks based on the stress distribution between fractures, which depends on the physical properties of neighbouring layers. The observations on our numerical models are that

1. at the onset of extension, many faults are nucleated in both modes.
2. when r_τ is small, many of the nascent fault zones are activated.
3. when r_τ is large, few fault zones are activated, but each accommodates large strain, leading to an *mcc* mode.

For a fractured layer sandwiched between two unfractured layers, *Bai and Pollard* [2000] find that there is a critical fracture spacing to layer thickness below which the interfracture stress is always compressive and new fractures will not form. At greater fracture spacings, the stress becomes tensile, and eventually overcomes the tensile strength of the layer, leading to new infill fractures. This critical spacing to

thickness ratio increases with increasing ratio of Young's modulus between the fractured and neighbouring layers. Although the *Bai and Pollard* [2000] analysis is for linear elastic media, we find an exact analogue in our results for normal faulting of viscoplastic layers. As the strength ratio r_τ increases, the spacing between active faults increases. Thus the magnitude of lateral stress transfer from the unfaulted lower crust to the upper crust is key to the mode of extension, where the mode is specifically controlled by the number of active fault zones. A relatively strong lower crust provides greater traction at the base of the upper crust, which results in the yield stress being reached at shorter spacings between faults. The existence of few fault zones in the presence of a weak lower crust is simultaneously linked to the ability of crustal blocks to rotate because of lower crustal mobility, leading to *mcc* formation.

The geometric origin of low-angle detachment faults remains controversial after years of research. According to *Scott and Lister* [1992] and *Livaccari et al.* [1995], for example, structural field relations favour initiation and activation at a shallow dip. Others such as *Buck* [1988] and *Wernicke and Axen* [1988] propose initial high-angle faults that subsequently rotate to shallow dip. In all of our simulations, initially high-angle normal faults form as planar features. They evolve to shallower angles because of lower crustal flow, or isostatic compensation, during unloading of the footwall. This rotation first manifests itself at the base of the upper crust, where the changes in the local stress field are greatest. The result is the slightly listric faults most evident in Figure 3a. Continued unroofing and lower crustal flow can eventually produce very shallow faults such as those around the *mccs* of Figure 5c. These results do not contradict the hypothesis that detachment faults are formed at low angle. There is simply no condition present for an initial stress field rotated from the vertical, and new faults form at 33° to σ_1 . However, the results do illustrate and support the hypothesis that initial high-angle faults can rotate to low angle and develop into shallow detachment faults that continue to slip due to significant weakening. It is worth noting a Coulomb failure analysis by *Wills and Buck* [1997] that determines the likelihood of fault slip at shallow dips due to specific boundary or loading conditions. They conclude that slip will not occur on low-angle surfaces unless there exists a questionable combination of localised, near-lithostatic pore pressure, and unsustainably high tensile stresses in the upper 5 km of the crust. On the other hand, if normal faults form at shallow dips because of pre-existing weaknesses, for example earlier shallow thrust faults [e.g., *Horvath*, 1993], vertical rheological strength contrasts are no longer as important in governing the mode of extension.

Through numerical experiments on a single elasto-plastic layer, *Lavier et al.* [2000] find that both the layer thickness and the amount of fault weakening can affect the degree of offset per fault. However, because the experiments are over an inviscid substrate, in all cases *Lavier et al.* [2000] nucleate a single fault zone only (this includes a single graben or horst with secondary faults in the same zone), i.e., the endmember of *mcc* mode. By including the important role of the lower crust in distributing stresses, we have determined fault weakening to be less important than the rheological contrast between upper and lower layers of the crust. Model D in Figure 6 suggests that significant differences in fault strength and rate of weakening change the characteristics of *mcc* formation, but not the actual mode of extension. Changes in relative layer thickness have a more pronounced effect, as indicated by the models with varying r_h in Figure 9. The critical value of r_τ for the transition between modes of extension varies inversely with the thickness of the lower crust, as explained above.

More sophisticated models by *Lavier and Buck* [2002] include a visco-elastic lower crust. While their purpose is to investigate the influence of cooling rate on faulting style, their models fit within our description of modes. Our estimated values of r_τ for the models presented by *Lavier and Buck* [2002] are all very high, such that they are well within *mcc* mode and consequently nucleate single fault zones, albeit sometimes composed of more than one individual fault.

Finally, we translate r_τ values into natural viscosity for the lower crust and compare with independent estimates. The distributed faulting mode, with $r_\tau = 0.53$, has a minimum lower crust viscosity of 9×10^{21} Pa·s. The *mcc* mode returns a viscosity of 3.9×10^{20} Pa·s. We have no estimates of crustal viscosity for western Turkey, but the *mcc* mode value is very close to the upper limit of 5×10^{20} Pa·s obtained by *Pollitz et al.* [2001], based on geodetic measurements of post-seismic velocity fields after the 1999 Hector Mine earthquake in California.

5 Conclusion

The primary rheological control on the mode of extension in the Earth's crust is the ratio of upper to lower crustal strength. This ratio dictates fault spacing through the stress transfer from ductile lower crust to brittle upper crust. The fault spacing, naturally linked to the ability of the lower crust to flow, then controls the subsequent evolution of the normal fault systems. Although pre-existing weaknesses are probably responsible for the initiation of many large detachment faults and metamorphic core complexes, a true mode of extension, which does not rely on large-magnitude initial heterogeneities to control fault spacing, is the result of vertical rheological contrasts. A small ratio of upper to lower crustal strength leads to a distributed mode of faulting, where many faults each take up limited strain, and the upper crust is never completely dissected. An example is faulting in the North Sea. A large strength ratio results in few active fault zones, each accommodating a large amount of strain. This leads to block rotation and complete dissection of the upper crust, with the consequent exhumation of lower crustal rocks. Examples of this mode of extension may be the metamorphic core complexes of the Western U.S.A. and the Aegean. The actual critical strength ratio for the transition between modes will depend upon such factors as the relative thickness of the lower crust with respect to the upper crust, and the degree of fault weakening. These are secondary factors that do not alter the primary importance of vertical rheological contrasts in determining the mode of extension.

References

- Axen, G., B. Wernicke, M. Skelly, and W. Taylor, Mesozoic and Cenozoic tectonics of the Sevier thrust belt in the Virgin River Valley area, southern Nevada, in *Basin and Range Extensional Tectonics Near the Latitude of Las Vegas, Nevada*, edited by B. Wernicke, vol. Memoir 176, pp. 123–153, Geological Society of America, Boulder, Colorado, 1990.
- Bai, T., and D. Pollard, Fracture spacing in layered rocks: a new explanation based on the stress transition, *Journal of Structural Geology*, 22, 43–57, 2000, doi:10.1016/S0191-8141(99)00137-6.

- Benes, V., and P. Davy, Modes of continental lithospheric extension; experimental verification of strain localization processes, *Tectonophysics*, 254, 169–87, 1996.
- Bird, P., and X. Kong, Computer simulations of California tectonics confirm very low strength of major faults, *Geological Society of America Bulletin*, 106, 159–174, 1994.
- Brace, W., and D. Kohlstedt, Limits on lithospheric stress imposed by laboratory experiments, *Journal of Geophysical Research*, 85, 6248–6252, 1980.
- Brun, J.-P., D. Sokoutis, and J. van den Driessche, Analogue modelling of detachment fault systems and core complexes, *Geology*, 22, 319–322, 1994.
- Buck, W., Flexural rotation of normal faults, *Tectonics*, 7, 959–973, 1988.
- Buck, W., Modes of continental lithospheric extension, *Journal of Geophysical Research*, 96, 20,161–20,178, 1991.
- Burchfiel, C., R. Nakov, T. Tzankov, and L. Royden, Cenozoic extension in Bulgaria and northern Greece: The northern part of the Aegean extensional regime, in *Tectonics and Magmatism in Turkey and the Surrounding Area*, edited by E. Bozkurt, J. Winchester, and J. Piper, vol. Special Publication 173, pp. 325–352, Geological Society, London, 2000.
- Byerlee, J., Brittle-ductile transition in rocks, *Journal of Geophysical Research*, 73, 4741–4750, 1968.
- Christiansen, P., and D. Pollard, Nucleation, growth and structural development of mylonitic shear zones in granitic rock, *Journal of Structural Geology*, 19, 1159–1172, 1997, doi:10.1016/S0191-8141(97)00025-4.
- Corti, G., M. Bonini, F. Innocenti, P. Manetti, and G. Mulugeta, Centrifuge models simulating magma emplacement during oblique rifting, *Journal of Geodynamics*, 31, 557–576, 2001.
- Duebendorfer, E., A. Sewall, and E. Smith, The Saddle Island detachment; an evolving shear zone in the Lake Mead area, Nevada, in *Basin and Range Extensional Tectonics Near the Latitude of Las Vegas, Nevada*, edited by B. Wernicke, vol. Memoir 176, pp. 77–97, Geological Society of America, Boulder, Colorado, 1990.
- Dunbar, J., and D. Sawyer, How preexisting weaknesses control the style of continental breakup, *Journal of Geophysical Research*, B94, 7278–7292, 1989.
- Fossen, H., and A. Rørnes, Properties of fault populations in the Gullfaks Field, northern North Sea, *Journal of Structural Geology*, 18, 179–190, 1996.
- Frank-Kamenetskii, D., *Diffusion and Heat Exchange in Chemical Kinetics*, Princeton University Press, Princeton, New Jersey, 1955, ?? pp.
- Gauthier, P., and J.-P. Brun, Crustal-scale geometry and kinematics of late-orogenic extension in the central Aegean (Cyclades and Evvia Island), *Tectonophysics*, 238, 399–424, 1994.

- Gessner, K., U. Ring, C. Johnson, R. Hetzel, C. Passchier, and T. GÜngör, An active bivergent rolling-hinge detachment system: Central Menderes metamorphic core complex in western Turkey, *Geology*, 29, 611–614, 2001.
- Handy, M., S. Wissing, and L. Streit, Frictional-viscous flow in mylonite with varied biminerale composition and its effect on lithospheric strength, *Tectonophysics*, 303, 175–191, 1999, doi:10.1016/S0040-1951(98)00251-0.
- Hauser, E., T. Gephart, T. Latham, L. Bown, S. Kaufman, J. Oliver, and I. Lucchitta, COCORP Arizona transect: Strong crustal reflection data, *Geological Society of America Bulletin*, 99, 833–844, 1987.
- Hetzel, R., U. Ring, C. Akal, and M. Troesch, Miocene NNE-directed extensional unroofing in the Menderes massif, southwestern Turkey, *Geological Society of London Journal*, 152, 639–654, 1995.
- Hodges, K., L. McKenna, and M. Harding, Structural unroofing of the central Panamint Mountains, Death Valley region, southeastern California, in *Basin and Range Extensional Tectonics Near the Latitude of Las Vegas, Nevada*, edited by B. Wernicke, vol. Memoir 176, pp. 377–388, Geological Society of America, Boulder, Colorado, 1990.
- Horvath, F., Towards a mechanical model for the formation of the Pannonian Basin, in *The Origin of Sedimentary Basins; Inferences from Quantitative Modelling and Basin Analysis*, edited by S. Cloetingh, W. Sassi, and F. Horvath, pp. 333–357, Elsevier, Amsterdam, 1993.
- Jones, C., B. Wernicke, G. Farmer, J. Walker, D. Coleman, L. McKenna, and F. Perry, Variations across and along a major continental rift: An interdisciplinary study of the Basin and Range province, western USA, *Tectonophysics*, 213, 57–96, 1992.
- Koyi, H., and A. Skelton, Centrifuge modelling of the evolution of low-angle detachment faults from high-angle normal faults, *Journal of Structural Geology*, 23, 1179–1185, 2001.
- Lachenbruch, A., and J. Sass, Models of extending lithosphere and heat flow in the Basin and Range province, in *Cenozoic Tectonics and Regional Geophysics of the Western Cordillera*, edited by R. Smith and G. Eaton, vol. Memoir 152, pp. 209–250, Geological Society of America, Boulder, Colorado, 1978.
- Lachenbruch, A., and J. Sass, Heat flow and energetics of the San Andreas fault zone, *Journal of Geophysical Research*, 85, 6185–6222, 1980.
- Lachenbruch, A., and J. Sass, Heat flow from Cajon Pass, fault strength, and tectonic implications, *Journal of Geophysical Research*, 97, 4995–5015, 1992.
- Lavier, L., and W. Buck, Half graben versus large-offset low-angle normal fault: Importance of keeping cool during normal faulting, *Journal of Geophysical Research*, 107, 2002, doi:10.1029/2001JB000513.

- Lavier, L., W. Buck, and A. Poliakov, Factors controlling normal fault offset in an ideal brittle layer, *Journal of Geophysical Research*, 105, 23,431–23,442, 2000.
- Livaccari, R. F., J. W. Geissman, and S. J. Reynolds, Large-magnitude extensional deformation in the South Mountains metamorphic core complex, Arizona; evaluation with paleomagnetism., *Geological Society of America Bulletin*, 107, 877–894, 1995.
- McKenzie, D., and D. Fairhead, Estimates of the effective elastic thickness of the continental lithosphere from bouger and free air gravity anomalies, *Journal of Geophysical Research*, B 102, 27,523–27,552, 1997.
- Moresi, L., H.-B. Mühlhaus, and F. Dufour, Viscoelastic formulation for modelling of plate tectonics, in *Bifurcation and Localization in Soils and Rocks*, edited by H.-B. Mühlhaus, A. Dyskin, and E. Pasternak, pp. 337–344, Balkema, Rotterdam, 2001.
- Moresi, L., F. Dufour, and H.-B. Mühlhaus, Mantle convection models with viscoelastic/brittle lithosphere: Numerical methodology and plate tectonic modeling, *Pure Appl. Geophysics*, 2002, in press.
- Moresi, L. N., and A. Lenardic, Three-dimensional mantle convection with continental crust: first-generation numerical simulations, *Earth Interactions*, 3, 1999.
- Mühlhaus, H.-B., H. Sakaguchi, L. Moresi, and N. Graham, Particle in cell and discrete element models for granular materials, in *Computer Methods and Advances in Geomechanics*, edited by C. Desai, T. Kundu, S. Harpalany, D. Contractor, and J. Kemini, pp. 511–518, Balkema, Rotterdam, 2001.
- Mühlhaus, H.-B., L. Moresi, B. Hobbs, and F. Dufour, Large amplitude folding in finely layered viscoelastic rock structures, *Pure Appl. Geophysics*, in press, 2002.
- Mulugeta, G., and W. Ghebreab, Modeling heterogeneous stretching during episodic or steady rifting of the continental lithosphere, *Geology*, 29, 895–898, 2001.
- Niemi, N., B. Wernicke, R. Brady, J. Saleeby, and G. Dunne, Magnitude and timing of extreme continental extension, central Death Valley region, California, in *Proceedings of Conference on Status of Geologic Research and Mapping, Death Valley National Park*, edited by J. Slate, vol. Open-File Report 99-0153, pp. 33–35, U.S. Geological Survey, Denver, Colorado, 1999.
- Parsons, T., J. McCarthy, and G. Thompson, Very different response to extreme extension in the southern Basin and Range and Colorado Plateau transition, vol. Publication 30, pp. 291–303, Utah Geological Association, 2000.
- Pollitz, F., C. Wicks, and W. Thatcher, Mantle flow beneath a continental strike-slip fault: Postseismic deformation after the 1999 Hector Mine earthquake, *Science*, 293, 1814–1818, 2001.
- Saunders, P., K. Priestley, and T. Taymaz, Variations in the crustal structure beneath western Turkey, *Geophysical Journal International*, 134, 373–389, 1998, doi:10.1046/j.1365-246x.1998.00571.x.
- Scott, R., and G. Lister, Detachment faults; evidence for a low-angle origin, *Geology*, 20, 833–836, 1992.

- Spencer, J., and S. Reynolds, Tectonics of mid-tertiary extension along a transect through west central Arizona, *Tectonics*, *10*, 1204–1221, 1991.
- Suppe, J., *Principles of Structural Geology*, Prentice-Hall, New Jersey, 1985, 537 pp.
- Viejo, G., M. Laigleb, and C. Raneroc, Pre-Permian sedimentary basins in the North Sea: images from reprocessed and pre-stack depth migrated MONA LISA data, *Marine and Petroleum Geology*, *19*, 519–526, 2002, doi:10.1016/S0264-8172(02)00030-2.
- Wernicke, B., Theory of large-scale, uniform-sense normal simple shear of the continental lithosphere, *Canadian Journal of Earth Science*, *22*, 108–125, 1985.
- Wernicke, B., and G. Axen, On the role of isostasy in the evolution of normal fault systems, *Geology*, *16*, 848–851, 1988.
- Wernicke, B., J. Spencer, B. Burchfiel, and P. Guth, Magnitude of crustal extension in the southern Great Basin, *Geology*, *10*, 499–503, 1982.
- Wills, S., and W. Buck, Stress-field rotation and rooted detachment faults: A Coulomb failure analysis, *Journal of Geophysical Research*, *102*, 20,503–20,514, 1997.
- Zoback, M., W. Prescott, and S. Krueger, Evidence for lower crustal ductile strain localization in southern New York, *Nature*, *317*, 705–707, 1985.

A Scaling

The following scaling factors are the ratio of natural to model parameter values, and contain the appropriate SI units. The model bounding box initially measures one dimensionless unit in height by two units in length, and represents a true system 160 km long. Comparison of natural versus model dimensions leads to a length scale

$$L^* = \frac{L_{\text{nature}}}{L_{\text{model}}} = 8 \times 10^4 \text{ m.}$$

A model boundary velocity of 1.0 translates into a strain rate of 0.5. The true strain rate of $6.3 \times 10^{-15} \text{ s}^{-1}$ results in a scale factor $\dot{\epsilon}^* = 1.26 \times 10^{-14} \text{ s}^{-1}$.

Equivalence of lithostatic versus viscous stresses demands that

$$\sigma^* = \rho^* g^* L^* = \eta^* \dot{\epsilon}^*$$

Both the gravitational and density scales g^* and ρ^* are equal to unity, so the resultant viscosity scale $\eta^* = 6.35 \times 10^{18} \text{ Pa}\cdot\text{s}$.

Matching the Peclet number $\text{Pe} = \dot{\epsilon} L^2 / \kappa$ for both systems, with a natural thermal diffusivity $\kappa = 10^{-6} \text{ m}^2$, yields $\kappa^* = 8 \times 10^{-5} \text{ m}^2$.

The true base temperature of 1200 °C and a model gradient from 0 to 1 imply a temperature scale $T^* = 1.2 \times 10^3 \text{ }^\circ\text{C}$.

B Viscosity at brittle-ductile transition

In order to create a continuous maximum shear stress profile as in Figure 2, the viscosity η_u at the brittle to ductile transition z_u must satisfy both the brittle yield equation (1) and the temperature-dependent viscosity equation (2).

$$\eta_u = \frac{\tau_{\text{yield}}(z_u)}{\dot{\epsilon}} = \eta_o e^{-cT(z_u)}$$

Having fixed the strain rate and both c_o and c_p , η_u is derived from equation (1) for the yield stress before any strain softening, noting that the total overburden pressure p is the lithostatic stress reduced by the extensional stress.

$$\begin{aligned} c_o + c_p (\rho_u g z_u - \eta_u \dot{\epsilon}) &= \eta_u \dot{\epsilon} \\ \eta_u &= \frac{c_o + \rho_u g z_u c_p}{(1 + c_p) \dot{\epsilon}} \end{aligned}$$

With the parameter values from Table 1, the transition viscosity $\eta_u = 2.75 \times 10^{22}$ Pa·s. The constants η_o and c control the viscosity profile through the ductile region, and are related through the equations above.

$$\begin{aligned} e^{-cT(z_u)} &= \frac{\eta_u}{\eta_o} \\ -c \frac{\partial T}{\partial z} z_u &= \ln \left(\frac{c_o + \rho_u g z_u c_p}{(1 + c_p) \eta_o \dot{\epsilon}} \right) \\ c &= - \left(\frac{\partial T}{\partial z} z_u \right)^{-1} \ln \left(\frac{c_o + \rho_u g z_u c_p}{(1 + c_p) \eta_o \dot{\epsilon}} \right) \end{aligned}$$

C Integrated crustal strength

Referring to Figure 2, the integrated strength τ_{int} of the crust is simply the area between 0 and the maximum shear stress. This maximum stress is defined by the yield envelope in the brittle zone (equation (1)), and by the viscous stress $\eta \dot{\epsilon}$ in the ductile zone. The crustal response to extension is defined by the ratio r_τ of the integrated strength of the upper crust (initially all brittle) to that of the lower crust (initially all ductile).

$$r_\tau = \frac{\tau_{\text{int}}^u}{\tau_{\text{int}}^l}$$

For the upper crust at the onset of extension,

$$\begin{aligned} \tau_{\text{int}}^u &= \int_0^{z_u} \tau_{\text{yield}} dz \\ &= c_o z_u + \frac{1}{2} z_u (\tau_{\text{yield}}(z_u) - c_o) \\ &= c_o z_u + \frac{1}{2} z_u \left(\frac{c_o + \rho g z_u c_p}{1 + c_p} - c_o \right) \\ &= \frac{z_u}{2} \left(c_o + \frac{c_o + \rho g z_u c_p}{1 + c_p} \right) \end{aligned}$$

Integrating the viscous stress profile for the lower crust at an initial constant strain rate,

$$\begin{aligned}
\tau_{\text{int}}^l &= \int_{z_u}^{z_l} \eta(T) \dot{\epsilon} dz \\
&= \dot{\epsilon} \int_{z_u}^{z_l} \eta_0 e^{-cT} dz \\
&= \dot{\epsilon} \int_{z_u}^{z_c} \eta_0 e^{-c \frac{\partial T}{\partial z} z} dz + \dot{\epsilon} \int_{z_c}^{z_l} \eta_0 e^{-c \frac{\partial T}{\partial z} z_c} dz \\
&= -\frac{\eta_0 \dot{\epsilon}}{c \frac{\partial T}{\partial z}} \left[e^{-c \frac{\partial T}{\partial z} z} \right]_{z_u}^{z_c} + \eta_0 \dot{\epsilon} e^{-c \frac{\partial T}{\partial z} z_c} (z_l - z_c) \\
&= -\frac{\eta_0 \dot{\epsilon}}{c \frac{\partial T}{\partial z}} \left[e^{-c \frac{\partial T}{\partial z} z_c} - e^{-c \frac{\partial T}{\partial z} z_u} \right] + \eta_0 \dot{\epsilon} e^{-c \frac{\partial T}{\partial z} z_c} (z_l - z_c)
\end{aligned}$$